Thermal Science and Engineering Progress 57 (2025) 103129

Contents lists available at ScienceDirect

Thermal Science and Engineering Progress

journal homepage: www.sciencedirect.com/journal/thermal-science-and-engineering-progress

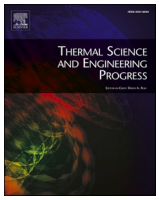

Heat and fluid flow analysis of micro-porous heat sink for electronics cooling: Effect of porosities and pore densities

Adeel Arshad [a,b,*], Muhammad Saeed [c], Muhammad Ikhlaq [d], Muhammad Imran [b], Yuying Yan [e]

[a] Environment and Sustainability Institute (ESI), Faculty of Environment, Science and Economy, University of Exeter, Penryn Campus, Cornwall TR10 9FE, United Kingdom
[b] Department of Mechanical, Biomedical and Design Engineering, Aston University, Birmingham B4 7ET, United Kingdom
[c] Abu Dhabi Maritime Academy, Abu Dhabi P.O. Box 54477, United Arab Emirates
[d] The Dyson Institute of Engineering and Technology, Malmesbury SN16 0RP, United Kingdom
[e] Fluids & Thermal Engineering (FLUTE) Research Group, Faculty of Engineering, University of Nottingham, Nottingham NG7 2RD, United Kingdom

ARTICLE INFO

Keywords:
Thermohydraulic Performance
Micro-porous heat sink
Heat and Fluid Flow

ABSTRACT

This investigation evaluates the hydrothermal efficiency of a micro-porous heat sink, utilizing water as a coolant and employing a single-phase model for analysis. The heat sink incorporates an aluminum metal foam as the micro-porous medium, with a focus on determining the optimal porosity (ε) and pore density (*PPI*) by examining variations within the ranges of $0.50 \leq \varepsilon \leq 0.90$ and $10 \leq \text{PPI} \leq 50$. This examination aims to delineate the effects of these variables on heat transfer and fluid flow characteristics. Assessment of thermal performance includes metrics such as log mean temperature difference (*LMTD*), average Nusselt number (Nu_{avg}), thermal resistance (R_{th}), volumetric flow rate (*Q*), pumping power (*PP*), overall performance (*OP*), and performance evaluation criteria (*PEC*). Additionally, fluid flow characteristics are analyzed through the examination of thermal contours and flow streamlines. Findings indicate that reducing ε from 0.90 to 0.50 and *PPI* from 50 to 10 yields superior Nu_{avg} and diminished R_{th} compared to conventional water-cooled micro-porous heat sinks. Notably, the most significant improvements in *LMTD* and R_{th} 83.04% and 61.44%, respectively, are observed with $\varepsilon = 0.50$ and $\text{PPI} = 30$ at a pressure drop (Δp) of 570 Pa. Consequently, $\varepsilon = 0.50$ and $PPI = 30$ are identified as the optimal parameters, achieving an enhancement of 396% compared to traditional non-porous heat sinks at the same pressure drop. This study recommends these parameters for achieving optimal thermohydraulic cooling performance in micro-porous, water-cooled heat sinks.

1. Introduction

The electronics industry faces increasing challenges due to overheating caused by the compactness of modern integrated circuit systems. This trend of miniaturization leads to higher heat generation in limited spaces, posing significant difficulties for thermal management [1]. Data centres, which are critical for global digital infrastructure, consume a substantial amount of electricity, with a significant portion dedicated to cooling systems [2]. The reliability of integrated circuits is notably affected by temperature, and overheating is a major cause of electronic component failure. Traditional cooling methods struggle to meet these demands. To date, many ways are being explored for heat dissipation including but not limited to; natural and forced convection [3], liquid forced convection [4,5], liquid boiling heat transfer [6], impingement cooling [7], spray cooling [8], two-phase cooling [9,10], Immersion cooling [11], and microchannel and micro heat sink cooling [12]. The limit to air cooling is around 100 W/cm^2, for high heat fluxes impingement and spray cooling are not recommended due to the complex configuration needed for these methods and limited by the degree of compactness needed [13]. Liquid cooling when combined with microchannel, micro pin–fin, and micro-porous heatsinks could be utilized for high heat fluxes and compact structures. In response, innovative cooling strategies have been explored, such as optimizing heat sink geometry and employing advanced coolants like metal-based nanofluids, supercritical CO_2, hybrid nanofluids, and porous micro heat sinks. These approaches aim to offer superior thermal conductivity and convective heat transfer rates to meet the thermal requirements of high-

* Corresponding author.
E-mail addresses: a.arshad@exeter.ac.uk, ia.arshad7@aston.ac.uk (A. Arshad).

https://doi.org/10.1016/j.tsep.2024.103129
Received 25 April 2024; Received in revised form 9 December 2024; Accepted 11 December 2024
Available online 15 December 2024

Nomenclature

Al	Aluminum
PPI	Pores per inch
PP	Pumping power
PEC	Performance evaluation criteria
OP	Overall performance
$LMTD$	Log mean temperature difference
L_{HS}	Length of heat sink
W_{HS}	Width of heat sink
H_{HS}	Height of heat sink
l_{mf}	Length of metal-foam
w_{mf}	Width of metal-foam
d_{out}	Outlet diameter
d_{in}	Inlet diameter
$\dot{Q}$	Heat transfer rate
$\dot{q}$	Heat flux
Q	Volumetric flow rate
Nu_{avg}	Average Nusselt number
R_{th}	Thermal resistance
t_{mf}	Thickness of metal-foam
Δp	Pressure drop
ω	Pore density
ε	Porosity

tech electronics [14].

In recent times, porous materials have also been employed due to their larger contact surface area and enhanced thermal efficiency in comparison to traditional fins [15,16]. Nevertheless, the pressure drops experience a significant increase when a porous medium is placed across the entire width of a channel with solid (non-porous) sidewalls. Essentially, this configuration hinders the flow along the length of the channel. This characteristic is anticipated to reduce the pressure drop when compared to a channel filled with a porous medium [17]. Consequently, a porous microchannel heat sink could be a suitable option for dissipating a substantial amount of heat in scenarios where high heat flux is generated, such as rocket engines, avionics, and fusion reactor blankets. Furthermore, the addition of nanoparticles to commonly used liquids (e.g., water or glycerine) in a heat sink might enhance the thermophysical properties and disrupt the formation of boundary layers [18].

Several research studies have demonstrated that the use of porous media can enhance the heat transfer capacity of a coolant in contact with a solid material [19,20]. As a result, scholars have explored the advantages of incorporating this method in Miniature Channel Heat Sinks (MCHSs) to enhance their efficiency [32–40]. Huang and Vafai [21] have examined the convective heat transfer of a porous block array configuration on an external surface. They have analyzed the impact of employing multiple porous block structures on fluid flow and heat transfer properties, considering various physical and geometric parameters through a stream function-vorticity transformation. The study delves into recirculation patterns, temperature field variations due to the porous medium, and the optimal arrangement for the porous matrix. Ould-Amera [22] investigated the use of a porous matrix between heat-generating blocks in a parallel plate channel. Their findings suggest that employing a porous medium significantly boosts the heat transfer rate. Furthermore, Huang and Vafai [23] explored heat transfer enhancement using alternative porous cavity-block wafers. They proposed an innovative approach to manipulate fluid flow and heat transfer on a surface by using porous cavity-block obstacles with different Reynolds, Darcy, and Prandtl numbers, as well as geometric parameters. Calmidi and Mahajan [24] conducted experimental and numerical investigations on forced convection in highly porous aluminium metal foams to gather Nusselt number data and determine empirical values for constants related to thermal dispersion and interfacial heat transfer coefficients across various porous samples. Yang and Hwang [25] implemented porous baffles at the top and bottom of rectangular channels to assess their influence on turbulent fluid flow and heat transfer properties. Their computational analysis revealed significant differences in flow patterns compared to solid baffles, indicating that porous baffles lead to lower friction factors while offering comparable heat transfer enhancement, especially for taller baffle heights.

Kau et al. [8] demonstrated the potential applications of open-cell metal foam for electronic cooling purposes. Meanwhile, Hunt et al. [26] conducted a study on the impact of intra-pore fluid mixing within the foam through forced convective heat transfer. Xu [27] provided a precise assessment of the thermal efficiency of porous media. When dealing with small duct scales and significant disparities in thermal conductivity between the solid and fluid, it is crucial to account for local thermal non-equilibrium (LTNE). Consequently, the subsequent study [28] investigated forced convection in a micro-channel partially filled with a porous medium under LTNE conditions. It was observed that fluid friction parameters decrease with higher Darcy and Knudsen numbers, as well as reduced porous media thickness. Despite being small in size, an open-cell metal foam heat sink is effective in dissipating heat from the CPU [29]. Nevertheless, maximizing heat dissipation in the processing unit can prove challenging due to various constraints like device size, materials, and current procedures. Therefore, exploring the impact of porosity in a micro-heat sink on enhancing thermal efficiency could be a valuable area of research, given the current limited understanding of this concept.

Extensive literature review highlights the importance of finding advanced thermal management solutions for electronic cooling. This involves exploring innovative materials and configurations like micro-porous metal foams and optimized coolant flows. However, there is a gap in understanding the relationship between the physical characteristics of micro-porous structures and their thermohydraulic performance. To address this gap, our study investigates the hydrothermal behavior of a micro-porous heat sink, which integrates an aluminum metal-foam with water as the coolant. Our aim is to identify the configurations that yield superior thermal resistance and heat transfer efficiency by examining the effects of varying pressure drops, porosity (ε), and pore density (PPI) on heat transfer and fluid flow dynamics. We apply varying pressure drops to discern the optimal ε and PPI values within specified ranges, thereby illuminating the intricate dependencies that govern the heat sink's performance.

This research stands out due to its rigorous methodology and innovative approach. This research innovatively combines a thorough examination of the effects of porosity (ε) and pore density (PPI) on the thermohydraulic performance of aluminum metal-foam heat sinks, using water as the coolant. By exploring a wide range of ε (0.50–0.90) and PPI (10–50) values with advanced numerical simulations, this study offers new insights into optimizing micro-porous heat sinks for superior thermal resistance and heat transfer efficiency. This comprehensive approach marks a significant advancement in electronic cooling solutions for high-heat-flux devices. The range of ε and PPI are chosen in such a way that the pressure drops are not significant, as this flow through individual pores is not modelled and not in the scope of this study. Advanced numerical simulations and a solid–fluid conjugate model guide this process. The research not only enhances our understanding of micro-porous heat sinks but also opens up new possibilities for optimizing the design and operation of these systems. The novelty of this work lies in its comprehensive examination of how ε and PPI work together to affect thermohydraulic efficiency. This represents a new

frontier in the optimization of micro-porous heat sink performance. The knowledge gained from this research has the potential to significantly contribute to the development of cooling solutions that can address the thermal management challenges posed by high-heat-flux electronic devices. This research is a significant step forward in the ongoing innovation of electronic cooling.

2. Numerical Formulation

2.1. Problem description

The physical representation of micro-porous heat sink computed in current study is shown in Fig. 1. The overall dimensions of heat sink are $L_{HS} = 21\ mm$, $W_{HS} = 18\ mm$ and $H_{HS} = 4\ mm$ with inlet and outlet diameter of $d_{in} = d_{out} = 2\ mm$ for circulating fluid inside the heat sink. An aluminium made micro-porous metal-foam having thickness of $t_{mf} = 2.5\ mm$ and $l_{mf} \times w_{mf} = 10 \times 10\ mm^2$ is embedded inside the heat sink, called micro-porous heat sink, with varying the porosity ($0.50 \leq \varepsilon \leq 0.90$) and pore density ($10 \leq PPI \leq 50$). A constant heat flux ($\dot{q}$) of 300 kW/m^2 was applied at heat sink base of $10 \times 10\ mm^2$ and pressure drop (Δp) was applied of 570 Pa $\leq \Delta p \leq$ 2760 Pa across the heat sink. A constant heat flux was supplied at the lower surface of the micro-porous heat sink, ensuring a steady and continuous flow of thermal energy. The constant flow of water is circulated inside the heat sink at ambient temperature. The thermophysical properties of heat sink, micro-porous metal-foam and coolant are provided in Table 1. In current study, an open-cell micro-porous metal-foam is considered which is formed from independent metal-foam ball, considered as the basic elemental unit of micro-porous metal-foam. The microstructure of micro-porous metal-foam adopted in current study is based on the physical model proposed by Boomsma and Poulikakos [30]. The three-dimensional microstructure and physical model generation of micro-porous metal-foam is illustrated in Fig. 2 [31,32].

Table 1
Thermophysical properties of materials [33,34].

Material	ρ (kg/m^3)	k (W/m.K)	μ (kg/m.s)	c_p (J/kg.K)
H_2O	997.1	0.613	0.00103	4179
Al	2719	202.37	–	871.0

2.2. Mathematical model

In order to accurately analyse and comprehend the convective flow and heat conduction processes that transpired within the micro-porous heat sink, the solid–fluid conjugate model was employed. This sophisticated model allowed for a comprehensive understanding of the intricate interplay between the solid structure of the heat sink and the fluid medium it interacts with. Moreover, the micro-porous medium of the heat sink was meticulously represented and accounted for by utilizing the Darcy-Forchheimer-Brinkman (DFB) momentum equation, which effectively captures the complex fluid dynamics taking place within the micro-porous heat sink [35,36].

The current problem considers the single-phase model in which fluid is modelled as a continuous phase in a three-dimensional (3D) micro-porous heat sink. There are some assumptions considered for numerical modelling:

(i) The flow is laminar, incompressible, single-phase, and steady state. At the pore lever, due to the pore size, a turbulent flow can be expected locally. Since individual pores are not modelled and not in the scope of this study.

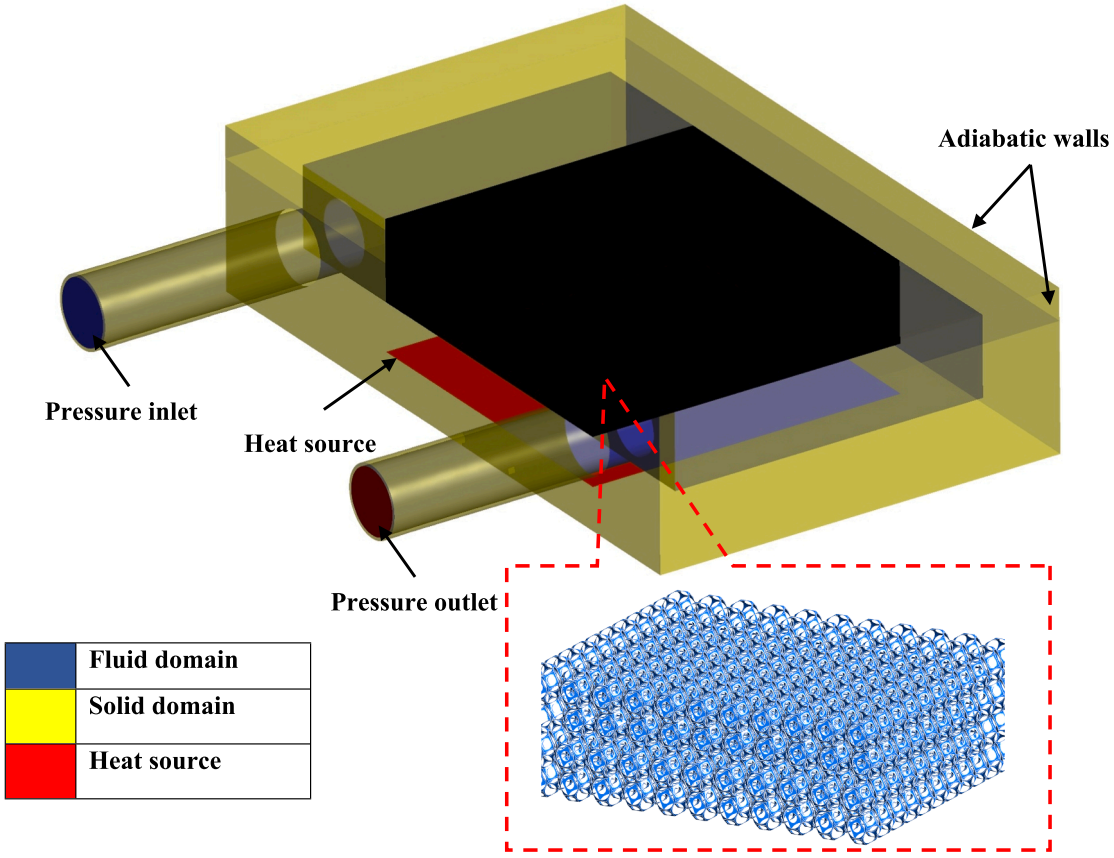

Fig. 1. Schematic micro-porous heat sink with boundary conditions.

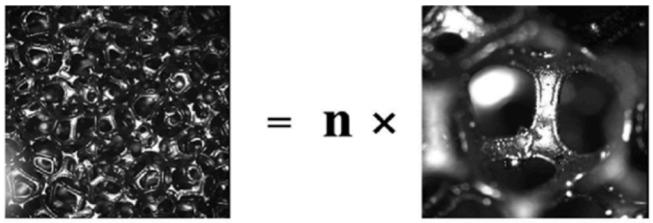

(a) Microstructure characterization of micro-porous metal-foam

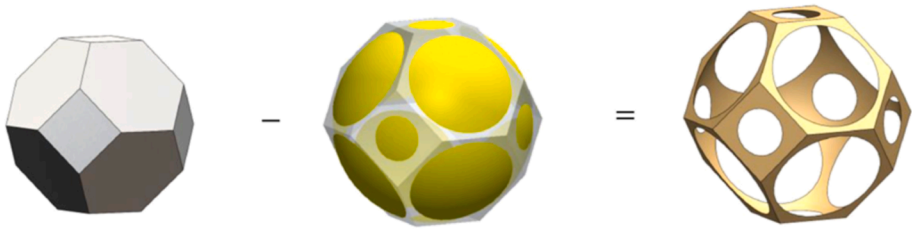

(b) Model generation procedure for micro-porous metal-foam.

Fig. 2. The microstructure and physical model generation procedure of micro-porous metal foam [28,29].

(ii) The thermophysical properties of the heat sink, porous media and fluid (the temperature difference from inlet to outlet for the fluid is less than 4 K) are assumed to be constant.
(iii) No-slip boundary conditions are considered for velocities. The radiative heat transfer and viscous dissipation are neglected, the Darcy-Forchheimer-Brinkman equation implicitly considers the viscous loss in the momentum equation.
(iv) The local thermal equilibrium (LTE) model is assumed between the micro-porous media, fluid, and heat sink domain in the energy equation.
(v) Interfacial losses between the fluid, micro-porous media, and heat sink are negligible.
(vi) The initial temperature and pressure conditions for heat sink, fluid and micro-porous media are the same.
(vii) The heat sink and micro-porous media are assumed to be considered in solid-state with homogenous and isotropic properties. An open cell micro-porous media is considered.

Consequently, by considering the above assumptions, the fundamental governing equations of mass conservation, momentum conservation, and energy conservation for the conjugate heat transfer problem can be written as follows [37]:

Mass conservation:

$$\nabla \cdot \mathbf{V} = 0 \tag{1}$$

Momentum conservation:

$$\frac{\rho_f}{\varepsilon}(\mathbf{V}.\nabla)\mathbf{V} = -\nabla p + \frac{\mu_f}{\varepsilon}\nabla^2\mathbf{V} + S_\phi \tag{2}$$

Energy conservation:

For fluid and micro-porous domain:

$$\left(\rho C_p\right)_f(\mathbf{V}.\nabla T) = k_{eff}\nabla^2 T \tag{3}$$

The effective thermal conductivity (k_{eff}) in Eq. (3) is introduced in LTE model which is calculated by volume averaging thermal conductivities of fluid (k_f) and micro-porous media (k_s) as follows:

$$k_{eff} = (1-\varepsilon)k_s + \varepsilon k_f \tag{4}$$

For solid domain:

$$k_s\nabla^2 T = 0 \tag{5}$$

In above Equations, 1–5, $\mathbf{V}$ denotes the velocity vector with u, v, and w, as the velocity components in x , y, and z directions. The p, μ_f, ρ_f, $C_{p,f}$ and T are the pressure, dynamics viscosity, specific heat capacity and temperature, respectively. The porosity ε is defined as the ratio between the void volume and the total volume of the micro heat sink. The ε is zero for non-porous walls and between 0 and 1 for porous wall. The source term S_ϕ in Eq. (2) is zero for non-micro-porous heat sink and defined by [38] for micro- porous wall.

$$S_\phi = -\left(\underbrace{\frac{\mu_f}{K_p}}_{\text{Darcy}}\mathbf{V} + \underbrace{\frac{\rho_f C_F}{\sqrt{K_p}}}_{\text{Forchheimer}}|\mathbf{V}|\,\mathbf{V}\right) \tag{6}$$

Here, the K_p and C_F are permeability and inertial coefficient, respectively. In Eq. (6), the right-hand side consists of Darcy and Forchheimer terms which refers to viscous loss and inertial loss terms, respectively. The Darcy terms consider the general porous resistance experienced by fluid while flowing through the porous media, whereas the Forchheimer term considers the inertial resistance occurred by the porous media as velocity or Reynolds number of fluid accelerates. The Brinkman coefficient (advective term along the porosity of porous media) takes into account the viscous resistance offered by the porous zone to fluid flow. The LTE model is assumed for heat transfer in fluid and solid porous substrate because of the fine pore size and higher thermal conductivity of porous substrate [39–41].

2.3. Micro-porous characterization

The geometric characteristics of micro-porous metal-foam are mainly dependent on the pore size and porosity of metal-foam which further define the other parameters such as permeability (K_p), inertial coefficient (C_F), etc. For a laminar incompressible flow regime driven by Δp, the K_p is a key parameter which defines the ability of fluid flow through porous media and depends on fluid velocity and pressure gradient. The K_p and C_F used in Eq. (6) are determined using the correlation proposed by Calmidi and Mahajan [24] as follows:

$$K_P = 0.00073(1-\varepsilon)^{-0.0024}\left(\frac{d_l}{d_p}\right)^{-1.11} d_p^2 \tag{7}$$

and

$$C_F = 0.00212(1-\varepsilon)^{-0.132}\left(\frac{d_l}{d_p}\right)^{-1.163} \tag{8}$$

The other parameters such porosity (ε), relative porosity (ε_r), cell or ligament diameter (d_l), pore size or pore diameter (d_p) and pore density (ω) which is the number of pores per inch (PPI), are also defined to describe the structure of metal-foam. These parameters are defined as follows [35,42]:

$$\varepsilon = \frac{V_v}{V_T} \tag{9}$$

$$\varepsilon_r = (1-\varepsilon) \tag{10}$$

$$d_l = d_p\left[1.18\sqrt{\frac{1-\varepsilon}{3\pi}}\left(\frac{1}{1-e^{-[(1-\varepsilon)/0.04)]}}\right)\right] \tag{11}$$

$$d_p = \frac{0.0245}{\omega(PPI)} \tag{12}$$

2.4. Boundary conditions

According to the reported experimental investigation [43], the pressure inlet and pressure out boundary conditions are applied at inlet and outlet of the heat sink, respectively. All solid–fluid interfaces and inner solid domains has been imposed as a no-slip boundary condition. Meanwhile, all outer domain wall except the heat source area and top lid of the heat sink are treated as adiabatic surfaces. The temperature of incoming fluid and pressure at the outlet of the heat sink are considered equivalent to the ambient conditions. Fig. 1 shows the schematic diagram of the computational domain.

2.5. Numerical procedure, grid analysis and validation

The current problem of conjugate heat transfer has been replicated through the utilization of the Finite Volume Method (FVM), a numerical technique for solving fluid flow and heat transfer problems, which has been implemented in a widely-used commercial software known as Ansys-FLUENT. The process of coupling the pressure and velocity components has been estimated and established through the employment of a coupled scheme, a method that ensures the accurate representation of the interaction between pressure and velocity. To discretize the pressure terms, a standard scheme has been utilized, which involves the division of the domain into control volumes and the application of suitable numerical approximations to the governing equations. On the other hand, the interpolation of the remaining parameters, which refers to the estimation of properties at intermediate locations within the computational domain, has been conducted through the implementation of the second-order upwind scheme, a numerical technique that provides improved accuracy and stability by considering the direction of flow and the associated numerical diffusion. The convergence criteria for all parameters (continuity, momentum, energy) have been limited to 10^{-05}. The grid topology study of used micro-porous heat sink is conducted extracting the results similar to Ikhlaq et al. [44] and variations are listed in Table 2 and presented in Fig. 3. The minimum percentage difference of 0.06% and 1.73% is obtain in T_{heater} and R_{th} between M4 and M5 grid size, respectively. Therefore, M4 mesh is selected for further simulations to reduce the convergence cost and to ensure the solution accuracy. Later, results were validated against the single-phase benchmark numerical [45] and experimental data [43], as shown in Fig. 4.

Table 2
Mesh independence study of water-cooled micro-porous heat sink.

Mesh	N_{cell}	T_{heater} (K)	Diff. (%)	R_{th}(K/W)	Diff. (%)
M1	909,385.00	310.650	0.45	0.422	11.64
M2	1,150,127.0	309.258	0.35	0.375	10.07
M3	1,561,923.0	308.179	0.09	0.339	2.68
M4	2,040,605.0	307.910	0.06	0.330	1.73
M5	2,382,293.0	307.740	–	0.325	–

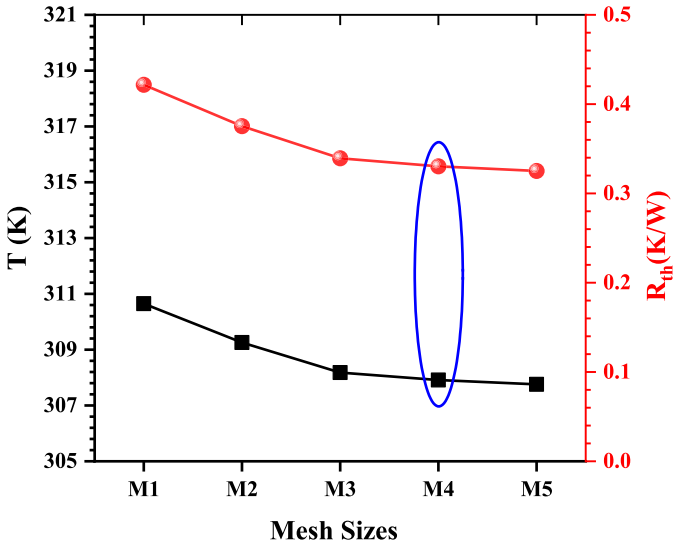

Fig. 3. Mesh independence results for different mesh sizes.

2.6. Performance evaluation parameters

The thermal hydraulic performance of micro-porous heat sink is determined by various parameters.

The thermal resistance (R_{th}) is calculated using Eq. (13) as follows [35,37]:

$$R_{th} = \frac{T_b - T_{in}}{\dot{Q}} \tag{13}$$

The average Nusselt number (Nu_{avg}) is obtained using average convective heat transfer coefficient (h_{avg}) and hydraulic diameter (d_h) of fluid flow as follows, Eq. (14) [46,47]:

$$Nu_{avg} = \frac{h_{avg} d_h}{k_f} \tag{14}$$

where, d_h and k_f are the hydraulic diameter and thermal conductivity of fluid, respectively. The h_{avg} is calculated using Eq. (15) as follows [36]:

$$h_{avg} = \frac{\dot{q}}{T_s - T_f} \tag{15}$$

where, $\dot{q}$ is the constant heat flux provided at the heat sink base. The T_f is the film temperature which is determined by averaging the inlet temperature (T_{in}) and outlet temperature (T_{out}) of fluid using Eq. (16), as follows [48]:

$$T_f = \frac{(T_{in} + T_{out})}{2} \tag{16}$$

The log mean temperature difference (*LMTD*), which considers the average temperature difference between the surface temperature of heat sink base and mean temperature of coolant at inlet, is calculated in Eq. (17), as follows [47]:

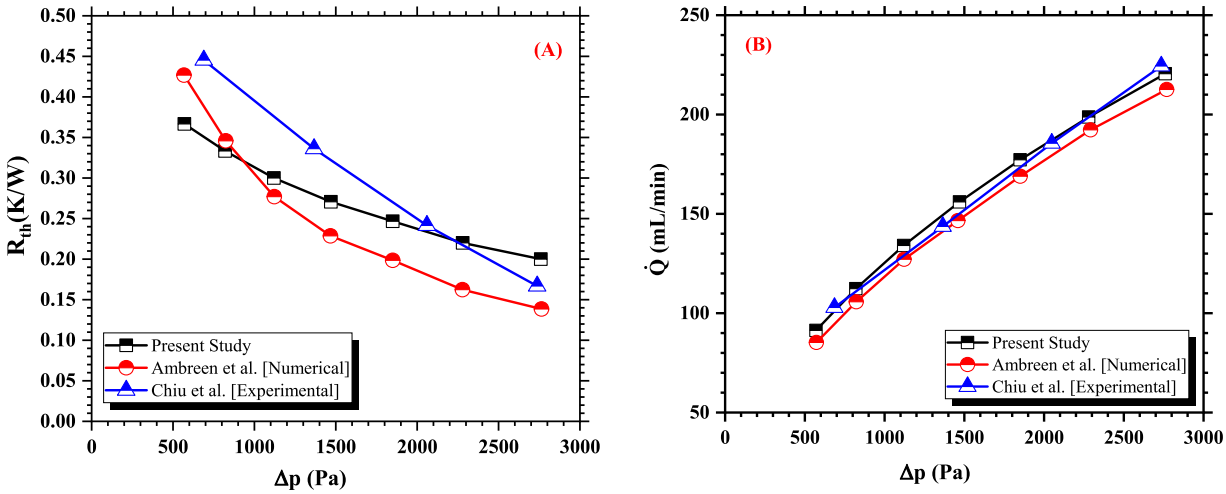

Fig. 4. Validation with experimental (Chiu et al. [43]) and numerical (Ambreen et al. [45]) studies for different Δp across the heat sink, (a) R_{th} and (b) Q.

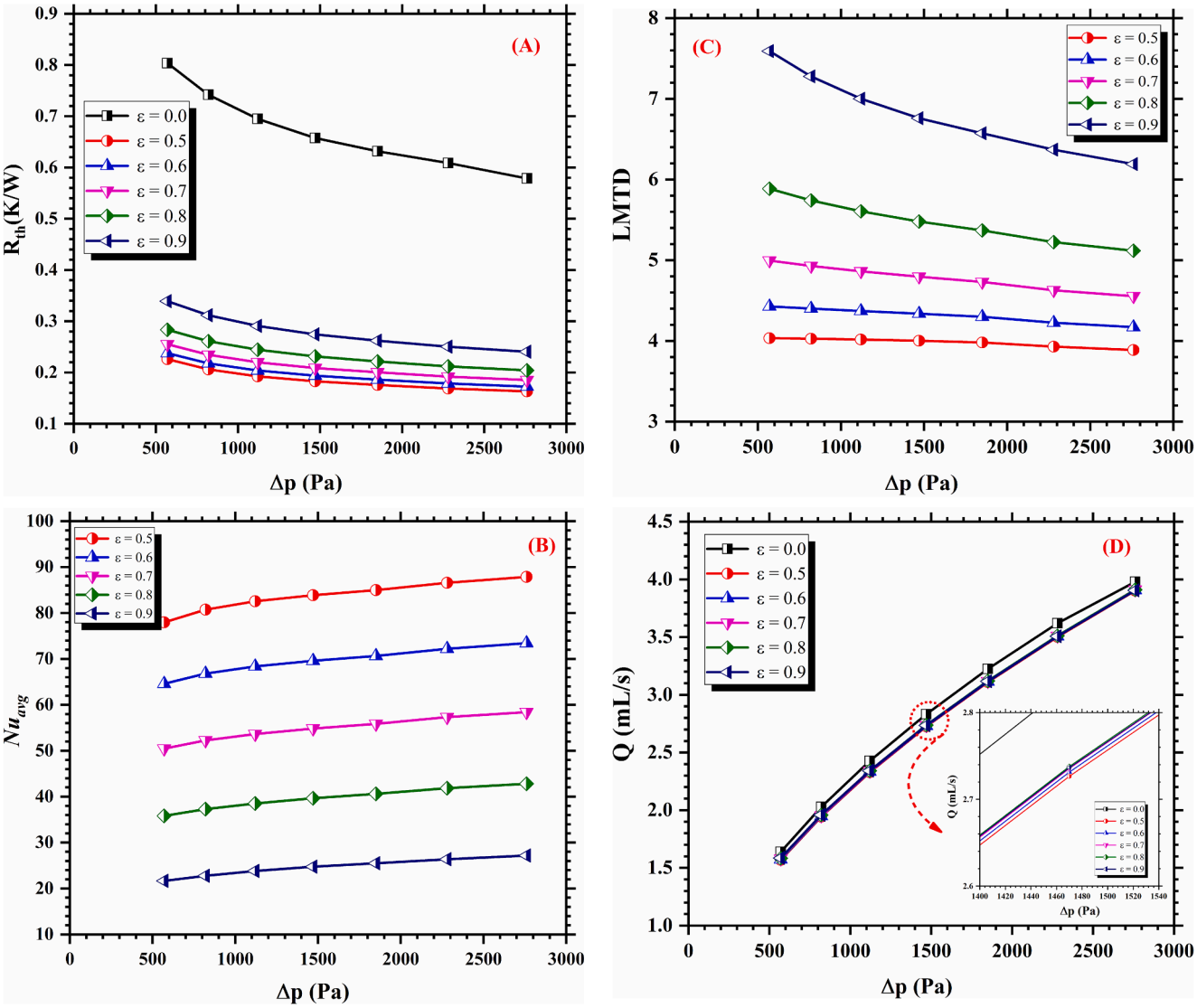

Fig. 5. Variation of (a) R_{th}, (b) Nu_{avg}, (C) LMTD, (D) Q, (E) PP, (F) OP and (G) PEC as a function of Δp for different ε.

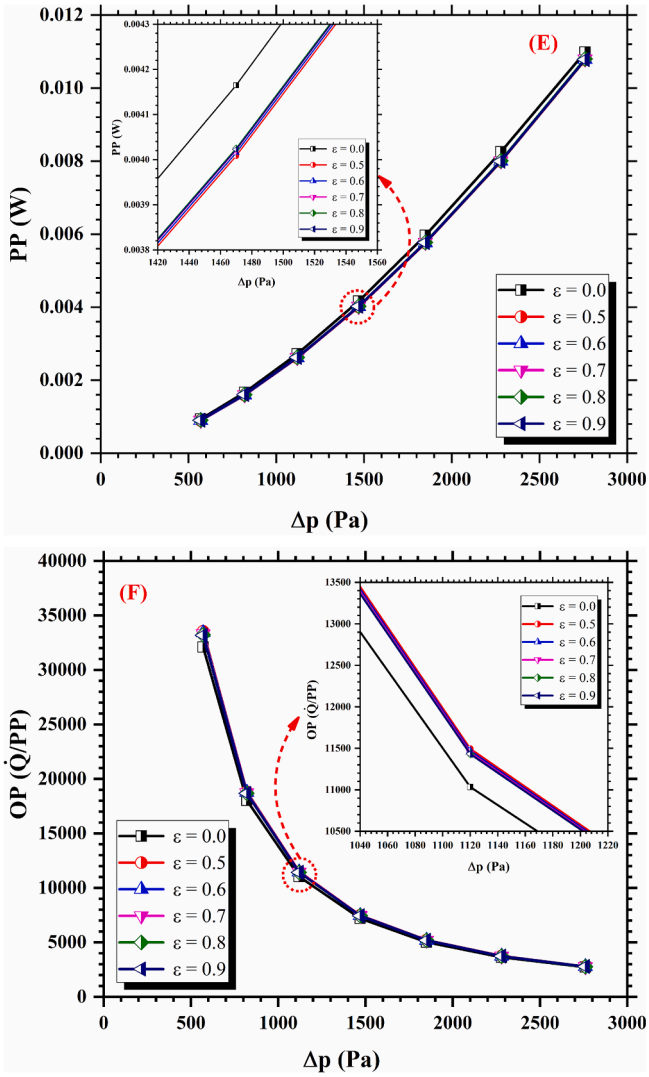

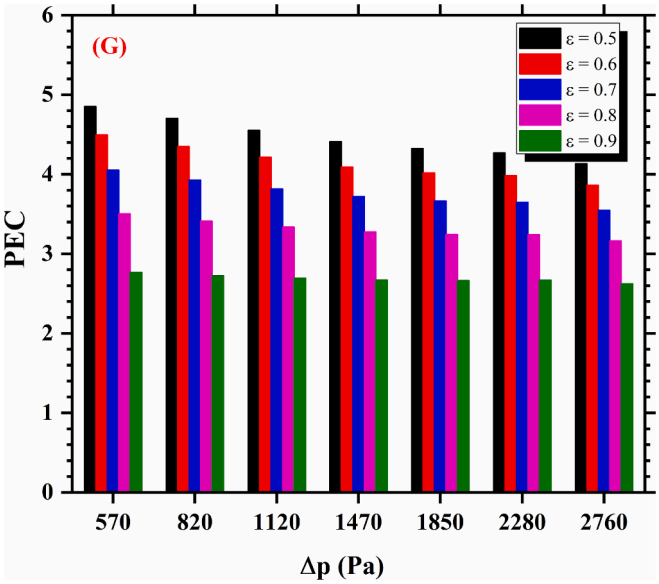

Fig. 5. (*continued*).

$$LMTD = \frac{(T_b - T_{in}) - (T_b - T_{out})}{\ln\left(\frac{T_b - T_{in}}{T_b - T_{out}}\right)} \tag{17}$$

The volumetric flow rate (Q) is calculated using Eq. (18) as follows [49]:

$$Q = \frac{v}{A_{avg}} \tag{18}$$

Where, v and A_{avg} are the average fluid velocity and average cross-sectional area of at the inlet of heat sink, respectively.

The pumping power (PP), which is required to pump the fluid across the heat sink, is computed using Q and Δp in Eq. (19), as follows [36]:

$$PP = Q \times \Delta p \tag{19}$$

The overall performance (OP) is evaluated by taking the ratio of heat transfer ($\dot{Q}$) and PP in Eq. (20), as follows [50]:

$$OP = \frac{\dot{Q}}{PP} \tag{20}$$

The performance evaluation criteria (PEC) is calculated using Eq. (21), as follows [36]:

$$PEC = \frac{Nu_{mf}/Nu_{wmf}}{\Delta p_{mf}/\Delta p_{wmf}} \tag{21}$$

where, the subscripts *mf* and *wmf* refer to the metal-foam and without metal-foam, respectively.

3. Results and discussion

3.1. Effect of varying porosity

The results of R_{th}, Nu_{avg}, $LMTD$, Q, PP, OP and PEC as function of Δp by varying two major geometric parameters of micro-porous media embedded in heat sink, ε and PPI, are shown in Fig. 5 and Fig. 6, respectively. Fig. 5A, illustrates the reduction in R_{th} with the decrease in ε from 0.90 to 0.50. A uniform reduction in R_{th} is observed by apply different Δp which shows the uniform heat distribution within the heat sink by using the micro-porous media of higher thermal conductivity compared to the without micro-porous media in case of $\varepsilon = 0.0$. A higher R_{th} is obtained without micro-porous media of around 0.80 K/W at $\Delta p =$ 570 Pa. The lowest R_{th} is obtained of between 0.226 to 0.163 K/W in case of $\varepsilon = 0.5$ by applying Δp from 570 Pa to 2760 Pa. It can be seen clearly that the variation in R_{th} results is not very significantly changing by using ε of 0.5, 0.6 and 0.7 especially operating at higher Δp conditions. However, this difference is uniformly and consistent, in case of

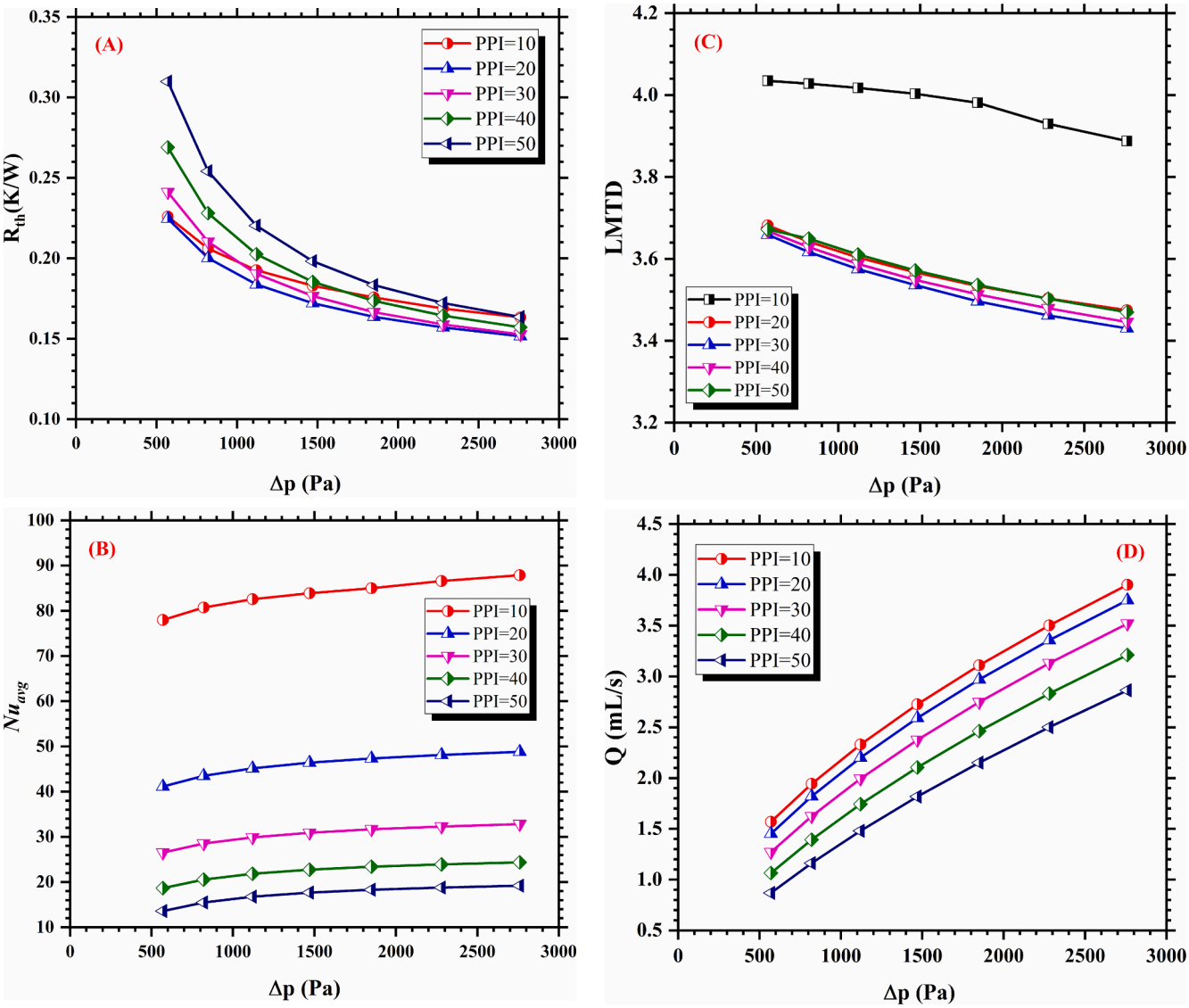

Fig. 6. Variation of (a) R_{th}, (b) Nu_{avg}, (C) LMTD, (D) Q, (E) PP, (F) OP and (G) PEC as a function of Δp for different PPI.

Nu_{avg} results, as shown in Fig. 5B, in case of all selected ε range and at each Δ*p*. The highest value of Nu_{avg} was obtained of 77.97 and 87.87 at Δ*p* of 570 Pa and 2760 Pa, respectively, by using a micro-porous media with ε = 0.50 and *PPI* = 10. The results of Nu_{avg} show that the increase in Nu_{avg} with the decrease of ε range is because of higher surface area of micro-porous media, hence the higher convective heat transfer rate. The lowest Nu_{avg} of 21.67 and 27.18 with ε of 0.90 at Δ*p* of 570 Pa and 2760 Pa, respectively.

Fig. 5C illustrates the variation of *LMTD* as a function of Δ*p* for variable ε. *LMTD* is also an important parameter to evaluate the thermal performance of heat sink which consider the average temperature difference between the surface temperature of heat sink base and mean temperature of coolant at inlet. *LMTD* and Nu_{avg} have the opposite trend to characterize the heat sink performance with increasing Δ*p* unlike the R_{th}. The decreasing trend in *LMTD* shows the more heat dissipation capacity of water-cooled micro-porous heat sink and lower values of *LMTD* are obtained upon decreasing of ε of micro-porous medium. The lowest decrease of 81.3% and 76.2% are obtained at Δ*p* of 570 Pa and 2760 Pa, respectively, in case of ε = 0.50 compared to the ε = 0.0. The comparison of *LMTD* of varying ε from 0.90 to 0.50 shows that lowest *LMTD* is achieved in case of ε = 0.50 followed by the 0.60, 0.70, 0.80 and 0.90 because of the more presence of micro-porous skeleton such as aluminium in present case, which resulted in higher surface area for heat augmentation. The lower values of *LMTD* shows the higher efficiency of micro-porous skeleton and heat dissipation capacity of fluid. In addition, increasing Δ*p* from 570 Pa and 2760 Pa, decreases the *LMTD* values of water-cooled micro-porous heat sink and augments the flow rate driven by the higher pressure gradient [51].

Fig. 5D presents variation of *Q* of coolant flowing through the micro-porous heat sink with the change of Δ*p* and increasing flow rate of fluid is obtained with the increase of Δ*p* for all porosities of micro-porous media. The increasing pressure gradient resulted in higher inlet velocity of fluid however, there is no significant variation in *Q* is observed with the change of ε from 0.50 to 0.90 which is because of constant pore density of *PPI* = 10, selected in present study. The results of *PP* as a function of Δ*p* for all cases of ε are shown in Fig. 5E. *PP* is an important parameter to investigate the thermal hydraulic performance of micro-porous heat sink which is the power being required to pump or circulate the coolant inside the heat sink. *PP* depends on the *Q* of coolant and Δ*p* across the heat sink. It is observed that *PP* augmented with the increase of Δ*p* however, the variation is not very significant because of the constant pore size for each ε from 0.50 to 0.90. In case of ε = 0.0, a slight

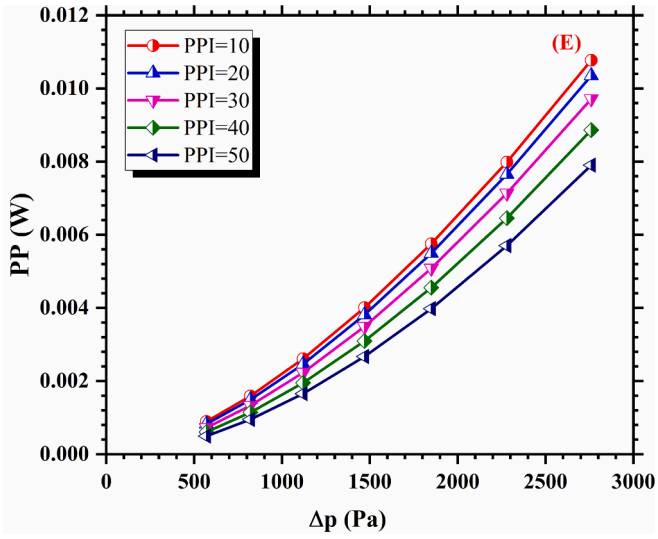

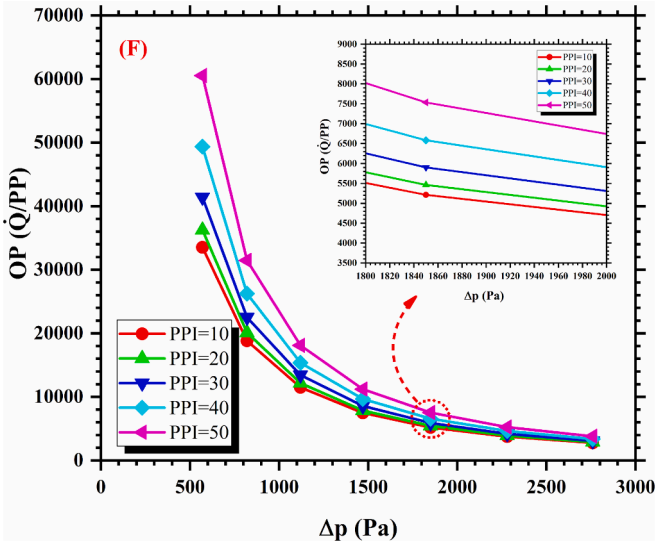

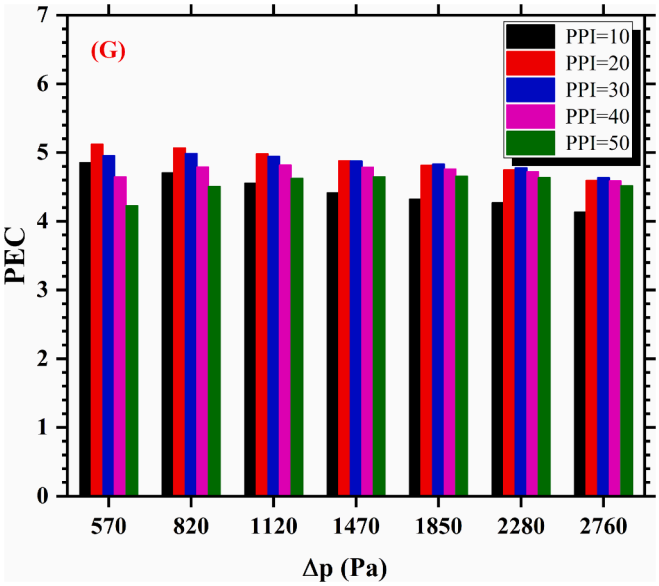

Fig. 6. (*continued*).

increase of 3.22% and 1.95 in *PP* is observed at Δ*p* of 570 Pa and 2760 Pa, respectively compared to the ε = 0.50.

The results of overall performance ($OP = \dot{Q}/PP$) of micro-porous heat sink is presented in Fig. 5F as a function of Δ*p* for all cases of ε. The *OP* is the ratio of $\dot{Q}$ and *PP* which simultaneously evaluates the effect of heat transfer and pumping power. It can be seen that there is no significant variation in *OP* results are observed by ε of micro-porous media at constant *PPI* which is because of constant pore size of metal-foam. However, it is revealed that *OP* decreases with the increase of Δ*p* because higher *PP* is required to flow the fluid at higher flow rate. A closer analysis reveals that a micro-porous media having ε of 0.5 has the better *OP* in comparison of all other ε of metal-foam.

The results of *PEC* of water-cooled micro-porous heat sink of varying ε are presented in Fig. 5G. *PEC* is defined as the ratio of convective heat transfer coefficient or Nusselt number and pressure drop therefore, it evaluates both positive and negative parameters. The higher value of *PEC* is obtained in case of ε = 0.50 for each Δ*p* followed by 0.60, 0.70, 0.80 and 0.90. The enhancement in *PEC* in case of ε = 0.50 compared to the ε = 0.0 or non-porous media, is obtained of 385% and 313% at Δ*p* of 570 Pa and 2760 Pa, respectively. Almost a linear decreasing trend can be seen for each ε of micro-porous media at a certain Δ*p* across the heat sink. Therefore, the results of Fig. 5 reveal that ε = 0.50 and *PPI* = 10 micro-porous heat sink shows the optimum and favourable thermohydraulic performance cooled with water.

3.2. *Effect of varying pore density*

In continuation of thermal performance analysis of micro-porous heat sink with water-cooled, the *PPI* of micro-porous media is explored from 10 to 50 at different Δ*p* for a constant of ε = 0.50. The results of R_{th} of different *PPI*, 10, 20, 30, 40 and 50, as a function of Δ*p* are shown in Fig. 6A. An interesting trend is observed that R_{th} decreased from 50 to 20 *PPI* exponentially. However, the R_{th} of *PPI* = 10 slightly increases from Δ*p* 820 Pa to 2760 Pa and reaches at the same level of *PPI* = 50 at Δ*p* of 2760 Pa. The exponential trend in the case of each *PPI* is because of the change in the pore size of micro-porous which increases the heat transfer area, hence heat transfer rate as well. The trend of Nu_{avg} of different *PPI* 10 to 50 is shown in Fig. 6B as a function of Δ*p*. The higher trend in Nu_{avg} is obtained in the case of 10 PPI at a constant ε of 0.50. The Nu_{avg} decreased with the increase of *PPI* in a constant trend from 10 to 50. The reduction trend Nu_{avg} in different *PPI* is because of the varying pore size of a single cell. A closer look reveals that by increasing the number of *PPI* the reduction in Nu_{avg} slightly decreases from the previous number of *PPI*. To explore the simultaneous effect of $\dot{Q}$ and *PP*, the *OP* is investigated for all cases of *PPI* operating at different Δ*p*.

The variation of *LMTD* for different *PPI* at constant ε of 0.50 as a

function of Δp, as shown in Fig. 6C. A decreasing trend in *LMTD* is achieved with the increase of Δp and lowest *LMTD* is obtained with a micro-porous media having *PPI* of 30 which shows the highest heat dissipation capacity with water as a coolant. A maximum decrease of 83.04% and 79.03% is achieved at Δp of 570 Pa and 2760 Pa, respectively, in case of $PPI = 30$ compared to the $PPI = 0$ or non-porous media. The variation in *LMTD* in case of 20 to 50 PPI is very slightly different especially at lower values of Δp.

Fig. 6D illustrates the results of Q of fluid flowing through the micro-porous heat sink by changing the *PPI* from 10 to 50 at varying Δp. The higher Q is achieved with the change of PPI at a certain Δp which means that velocity increases with the increase of Δp across the heat sink. However, at a constant Δp such as $\Delta p = 570$ Pa, the Q decreases with the increase of *PPI* from 10 to 50 at constant of $\varepsilon = 0.50$ because of the change of pore size diameter as well as the ligament diameter. As, pore density is changing from lower to higher ligament diameter therefore, fibre size increases or cell size decreases which resists the flow of fluid resulted in reduced the fluid flow velocity resulted in reduced the Q of coolant. The lowest reduction in Q is achieved of 46.95% and 28.14% at Δp of 570 Pa and 2760 Pa, respectively, in case of $PPI = 50$ compared to $PPI = 0$ micro-porous heat sink.

To qualify the required power to circulate the fluid or coolant inside the heat sink a certain Q, the results of *PP* are depicted in Fig. 6E. As the Q of flowing fluid is lower at higher *PPI* thus, lower *PP* is required at a certain Δp. The *PP* for 50 *PPI* is reduced of 46.24% and 28.05% compared to $PPI = 0$ at Δp of 570 Pa and 2760 Pa, respectively. However, in case of PPI = 10, the reduction in *PP* is obtained of 4.30% and 1.91% at Δp of 570 Pa and 2760 Pa, respectively. It reveals that with the increase of *PPI*, the *PP* is reduced similar to the Q with the increase of Δp across the micro-porous heat sink. As, the analysis of solely *PP* and Q are not enough to optimize thermal hydraulic performance of micro-porous heat sink by varying the $10 \leq PPI \leq 50$ at constant ε of 0.50, thus effect simultaneous effect of *PP* and $\dot{Q}$ is evaluated by *OP*.

The *OP* decreases exponentially for was each *PPI* lower to high value of Δp, as shown in Fig. 6F. It reveals a micro-porous heat sink operates at lower flow rate exhibits the higher thermohydraulic performance. The higher value of *OP* is obtained in case of 50 *PPI* at lower Δp of 570, 820 and 1120 Pa and a slight variation in *OP* is observed further applying the Δp from 1470 to 2760 Pa in comparison of other selected *PPI*. Like Nu_{avg} results for different *PPI*, a similar trend in reduction in *OP* results are observed for different *PPI* against varying Δp. The reduction in *OP* of two consecutive *PPI*, such as 50–40 or 40–30, is lower than the next two consecutive *PPI* especially at lower Δp of 570, 820 and 1120 Pa. The percentage in reduction of *OP* is very negligible at higher Δp or higher flow rate which requires higher *PP*.

Finally, the comparison of *PEC* for all *PPI* from 10 to 50 as a function of Δp is illustrated in Fig. 6G. As *PEC* contributes the simultaneous effect of Nu_{avg} and Δp and an interesting finding is revealed that higher *PEC* of 5.12, 5.07, and 4.98 is obtained for $PPI = 20$ at Δp of 570, 820, and 1120 Pa, respectively, whereas at Δp of 1470, 1850, 2280, and 2760 Pa the higher *PEC* of 4.83, 4.78 and 4.63, respectively, is obtained in case of $PPI = 30$. In addition, a close look reveals that *PEC* slightly decreases with the increase of Δp for *PPI* of 10 and 20. In case of $PPI = 30$, the maximum enhancement of 396% and 399% at Δp of 570 Pa and 820 Pa, respectively, compared to the $PPI = 0$ or non-porous media embedded heat sink. However, the maximum enhancement of 412% and 407% at Δp of 570 Pa and 820 Pa, respectively, is achieved in case of$PPI = 20$ compared to the $PPI = 0$. As mentioned earlier, the PEC increases at higher Δp across the heat sink at $PPI = 30$, therefore the optimum $PPI = 30$ is recommended for a micro-porous media.

In addition, the results of R_{th}, Nu_{avg}, *LMTD*, Q, *PP*, *OP* and *PEC* of different ε and *PPI* of micro-porous media, shown in Figs. 5 and 6, respectively, reveals the optimum value of ε and *PPI* of 0.50 and 30 operating at lower Δp or flow rates of coolant which gives the optimal thermal cooling performance.

3.3. Velocity, streamlines, temperature contours

The velocity contours at different *x-z* planes and flow streamlines across the micro-porous heat sink at a Δp of 570 Pa are shown in Fig. 7. The streamlines show the uniform and well-aligned distribution of fluid through the porous media which causes the high flow resistance and suppresses the fluid mixing. However, the large eddies and recirculation of fluid are observed at the inlet header because of high inlet fluid velocity. At the outlet header, fluid exits uniformly passing through the porous media. The uniform distribution and fluid mixing because the micro-porous media having higher thermal conductivity enhances the heat transfer rate and as a result enhances thermal cooling efficiency. The temperature distribution of fluid across the *x-y* and *x-z* planes along with the isometric view of heat sink are shown in Fig. 8. The lower temperature is observed at the inlet header and at the top of the heat sink along the micro-porous heat sink. In addition, a micro-porous heat sink uniformly distributes the heat from the heat sink base towards the top of heat sink. The local pressure distribution is illustrated in Fig. 9 along the *x-y* and *x-z* planes at different locations of micro-porous heat sink at a Δp of 570 Pa for the case of $\varepsilon = 0.50$ and $PPI = 30$. A higher pressure exhibits at the inlet header of the heat sink and along the heat sink toward the outlet header, a decreasing trend in pressure distribution is exhibited. The higher pressure at the inlet header of heat sink is because of the porous-fluid interface, however, the decreasing pressure towards the downstream of heat sink is because of the fully developed flow inside the porous zone and existing of fluid at the interface of flow-porous interface.

4. Conclusion

The current numerical study explored the effects of two major geometric parameters of micro-porous media such as ε and *PPI* in a range of $0.50 \leq \varepsilon \leq 0.90$ and $10 \leq PPI \leq 50$, respectively, at different pressure drops (Δp) boundary conditions at inlet and outlet of a water-cooled micro-porous heat sink. The heat and fluid flow characteristic of coolant was investigated by changing the ε and *PPI*. A uniform heat distribution and laminar flow phenomenon was observed at different flow conditions. The key findings and suggestions of this study are highlighted as follows:

- The thermal resistance (R_{th}) diminishes as the porosity (ε) decreases and the pore density (*PPI*) increases across various Δp. Notably, a substantial decrease in R_{th}, reaching a maximum of 71.89%, is observed at a Δp of 570 Pa when ε is set to 0.50 and *PPI* to 10. Conversely, with the same porosity of $\varepsilon = 0.50$ but at a higher *PPI* of 30, the reduction in R_{th} is slightly less, achieving a 61.44% decrease. This variation underscores the significant impact of pore density, in addition to porosity, on enhancing the heat sink's thermal performance under different operational conditions.
- The average Nusselt number (Nu_{avg}) experiences an upsurge as porosity (ε) diminishes and pore density (*PPI*) transitions from higher to lower values, specifically from 0.90 to 0.50 for ε and 50 to 10 for *PPI*. Notably, the peak Nu_{avg} values recorded are 87.87 at a Δp of 570 Pa and 79.97 at a Δp of 2760 Pa, both achieved with a configuration of $\varepsilon = 0.50$ and $PPI = 10$. Nonetheless, the variation in Nu_{avg} becomes less pronounced as *PPI* increases from 20 to 50, particularly when contrasted with the change observed between *PPI* values of 10 to 20. An optimal Nu_{avg} of 26.54 and 32.83, for Δp values of 570 Pa and 2760 Pa, respectively, is identified under conditions of $\varepsilon = 0.50$ and $PPI = 30$. This suggests a nuanced relationship between *PPI* and the heat transfer efficiency, highlighting the importance of optimizing both porosity and pore density to achieve superior thermal performance.
- The comparison of the log mean temperature difference (*LMTD*) across different porosity (ε) levels reveals that a lower *LMTD* is

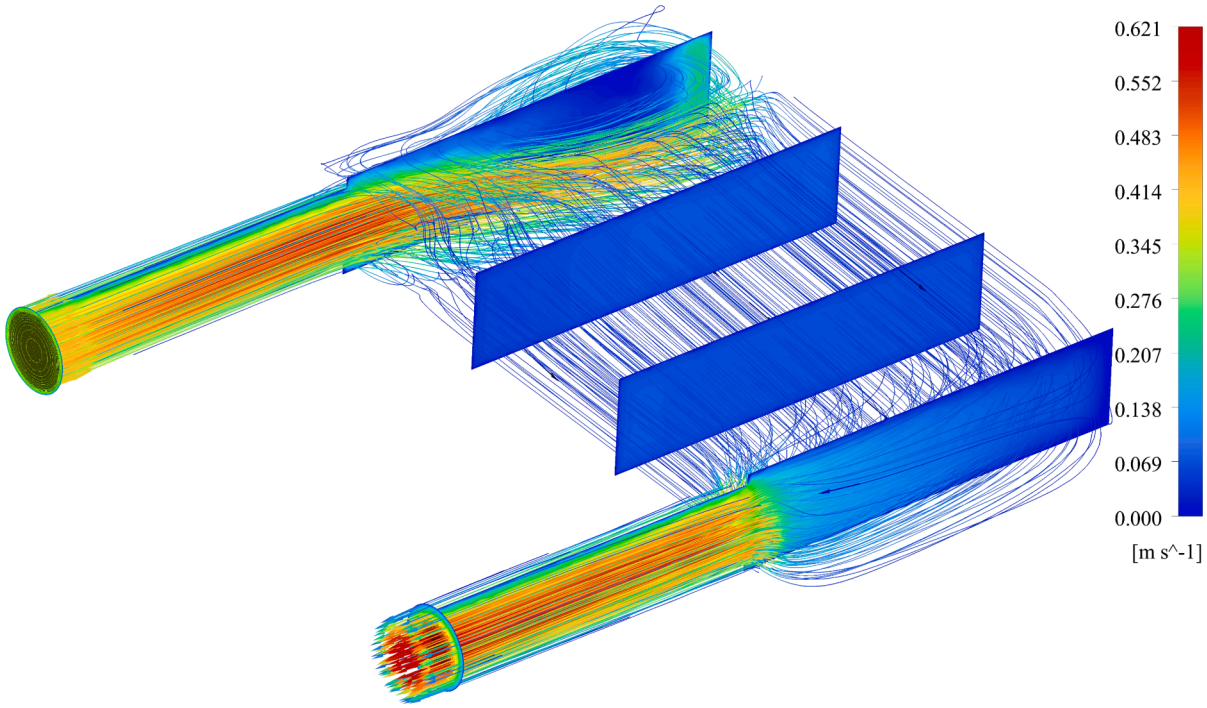

Fig. 7. Velocity contours and flow streamline of fluid across the heat sink at$\Delta p = 570$ Pa for $\varepsilon = 0.50$ and PPI = 30.

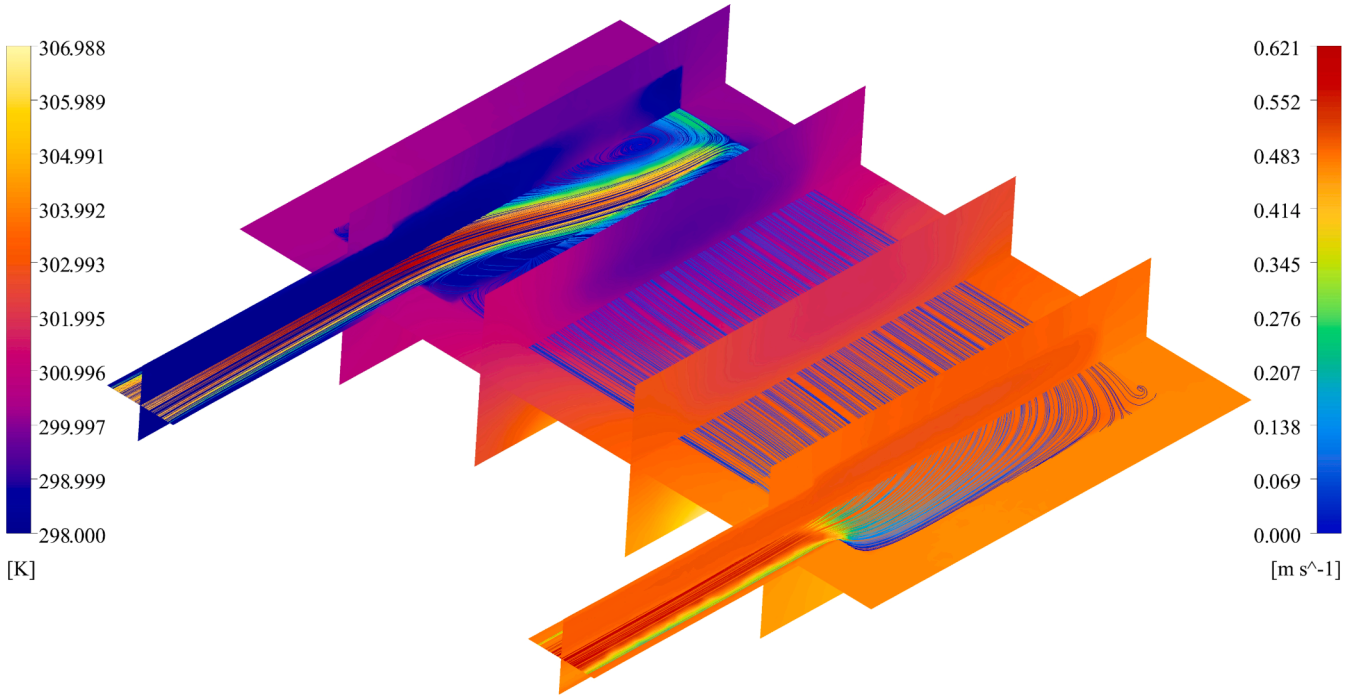

Fig. 8. Temperature contours and flow streamline at different x-y and x-z planes of microporous heat sink at$\Delta p = 570$ Pa for $\varepsilon = 0.50$ and PPI = 30.

achieved at $\varepsilon = 0.50$ and $PPI = 10$, witnessing a significant reduction of 81.3% and 76.2% for Δp values of 570 Pa and 2760 Pa, respectively. However, upon adjusting the pore density (*PPI*) from 10 to 50, while maintaining a constant ε of 0.50, the most substantial decrease in *LMTD* is observed with $\varepsilon = 0.50$ and $PPI = 30$, where reductions of 83.04% and 79.03% are recorded at Δp values of 570 Pa and 2760 Pa, respectively. This indicates that optimizing both porosity and pore density to specific values can significantly enhance the thermal performance of the heat sink, underscoring the critical balance between these two parameters for achieving optimal heat dissipation efficiency.

- The results of *Q*, *PP* and *OP* by changing the different ε at constant $PPI = 10$ show that *Q* and *PP* are increased with increase of Δp however, *OP* is decreased with increase of Δp. In addition, there is no significant change in observed in *Q*, *PP* and *OP* by varying the ε at constant *PPI* because of the constant pore size diameter of the microporous resulted in constant flow velocity of fluid is achieved. However, by changing the *PPI* from 10 to 50 at constant $\varepsilon = 0.50$, the

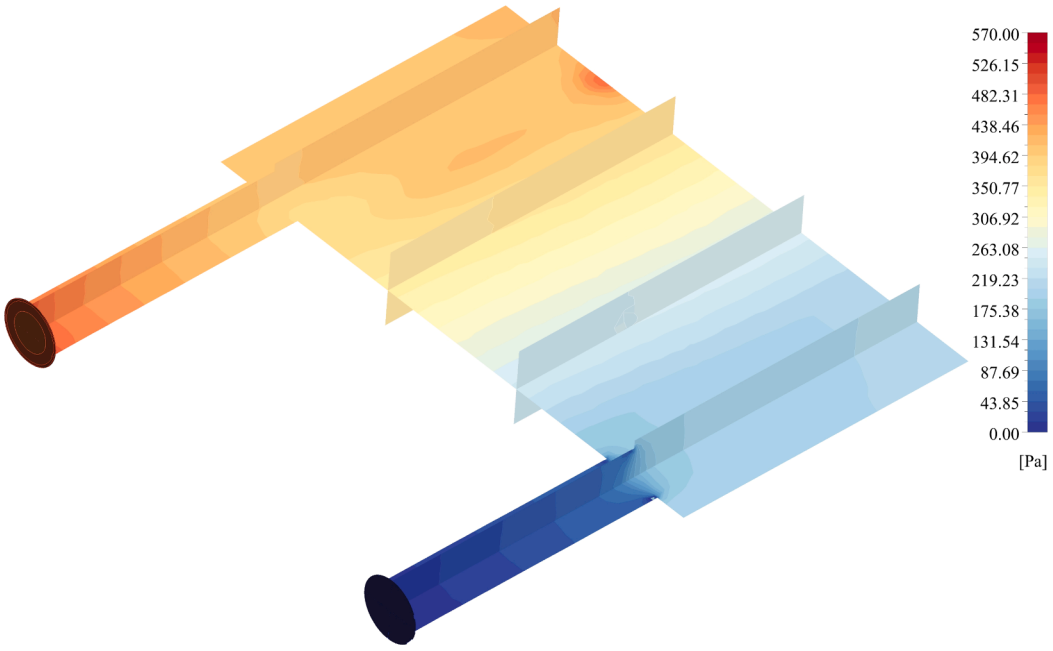

Fig. 9. Local pressure contours at different x-y and x-z planes of microporous heat sink at Δp = 570 Pa for ε = 0.50 and PPI = 30.

results of *Q*, *PP* and *OP* reveals the significance characteristics in *Q*, *PP* and *OP* because of different pore size diameter, and optimum ε and PPI is revealed of 0.50 and 30, respectively.

- The evaluation of performance evaluation criteria (*PEC*) across varying porosities (ε) and pore densities (*PPI*) reveals that significant enhancements in PEC, by 385% and 313%, are observed at pressure drops (Δ*p*) of 570 Pa and 2760 Pa, respectively, when ε is set to 0.50 and *PPI* to 10. However, adjusting *PPI* from 10 to 50, while keeping ε constant at 0.50, results in even greater enhancements. Specifically, PPIs of 20 and 30 achieve *PEC* improvements of 412% and 396%, respectively, at Δ*p* of 570 Pa. Moreover, as the pressure drop increases, the most substantial increase in *PEC* is observed with *PPI* = 30, underlining this configuration as the optimal choice for microporous media. This analysis underscores the nuanced interplay between porosity, pore density, and operational conditions in maximizing the thermal efficiency of micro-porous heat sinks, recommending a pore density of 30 as the most effective for enhancing heat sink.

The bottom line from the discussed conclusions highlights the critical influence of porosity (ε) and pore density (*PPI*) on the thermal performance of micro-porous heat sinks using water as a coolant. Specifically, an optimal configuration of ε = 0.50 and *PPI* = 30 emerges as the most effective for enhancing heat transfer efficiency, reducing thermal resistance, and improving the performance evaluation criteria (*PEC*) across varying pressure drops. This optimal setting not only achieves significant reductions in the log mean temperature difference (*LMTD*) but also maximizes the average Nusselt number (Nu_{avg}), underscoring the nuanced balance between porosity and pore density in optimizing the thermohydraulic efficiency of micro-porous heat sinks. These findings provide a clear direction for the design and operation of cooling systems in high-heat-flux applications, suggesting that careful adjustment of these parameters can lead to superior cooling performance.

CRediT authorship contribution statement

Adeel Arshad: Writing – original draft, Visualization, Validation, Software, Project administration, Methodology, Formal analysis, Data curation, Conceptualization, Writing – review & editing. **Muhammad Saeed:** Project administration, Supervision, Visualization, Writing – review & editing. **Muhammad Ikhlaq:** Project administration, Supervision, Visualization, Writing – review & editing. **Muhammad Imran:** Project administration, Supervision, Visualization, Writing – review & editing. **Yuying Yan:** Writing – review & editing, Visualization.

Declaration of competing interest

The authors declare that they have no known competing financial interests or personal relationships that could have appeared to influence the work reported in this paper.

Acknowledgments

This research is facilitated by the Faculty of Environment, Science and Economy, University of Exeter, UK and Department of Mechanical, Biomedical and Design Engineering, Aston University, Birmingham, UK research infrastructures. "*For the purpose of open access, the author has applied a Creative Commons Attribution (CC BY) licence to any Author Accepted Manuscript version arising from this submission*".

Availability of Data and Material.

There is no associated data with this article.

Data availability

The authors do not have permission to share data.

References

[1] W. Duangthongsuk, S. Wongwises, A comparison of the heat transfer performance and pressure drop of nanofluid-cooled heat sinks with different miniature pin fin configurations, Exp. Therm Fluid Sci. 69 (2015) 111–118.
[2] M. Ikhlaq, M. Yasir, M. Demiroğlu, M. Arik, Synthetic Jet Cooling Technology for Electronics Thermal Management—A Critical Review, IEEE Trans. Compon. Packag. Manuf. Technol. 11 (8) (2021) 1156–1170.
[3] G. Xie, B. Sundén, L. Wang, E. Utriainen, Parametric study on heat transfer enhancement and pressure drop of an internal blade tip-wall with pin-fin arrays, Heat Mass Transf. 47 (1) (2011) 45–57.
[4] E. Baker, Liquid cooling of microelectronic devices by free and forced convection, Microelectron. Reliab. 11 (2) (1972) 213–222.

[5] B.X. Wang, X.F. Peng, Experimental investigation on liquid forced-convection heat transfer through microchannels, Int. J. Heat Mass Transf. 37 (1994) 73–82.
[6] O.A. Alawi, N.A.C. Sidik, H.A. Mohammed, S. Syahrullail, Fluid flow and heat transfer characteristics of nanofluids in heat pipes: A review, Int. Commun. Heat Mass Transfer 56 (2014) 50–62.
[7] M. Ikhlaq, Y.M. Al-Abdeli, M. Khiadani, Flow and heat transfer characteristics of turbulent swirling impinging jets, Appl. Therm. Eng. 196 (2021) 117357.
[8] W.-L. Cheng, W.-W. Zhang, H. Chen, L. Hu, Spray cooling and flash evaporation cooling: The current development and application, Renew. Sustain. Energy Rev. 55 (2016) 614–628.
[9] Ghaffari, O., Vincent, M., Grenier, F., Larimi, Y. N., Jasmin, S., Fréchette, L., and Sylvestre, J., "Pushing the Limits of Air Cooling with Novel Two-Phase Prototypes for High Power Microprocessors," Proc. 2023 22nd IEEE Intersociety Conference on Thermal and Thermomechanical Phenomena in Electronic Systems (ITherm), pp. 1-6.
[10] M. Vincent, O. Ghaffari, Y. Nabavi Larimi, F. Grenier, S. Jasmin, L. Fréchette, J. Sylvestre, Experimental investigation of the thermal resistance of advanced two-phase thermosyphon heatsinks, Appl. Therm. Eng. 238 (2024) 122108.
[11] Larimi, Y. N., Ghaffari, O., Ganjali, A., Sayed, C. A., Grenier, F., Jasmin, S., Fréchette, L., and Sylvestre, J., "Multi-Scale Electroplated Porous Coating for Immersion Cooling of Electronics," Proc. 2022 21st IEEE Intersociety Conference on Thermal and Thermomechanical Phenomena in Electronic Systems (iTherm), pp. 1-7.
[12] N.A.C. Sidik, M.N.A.W. Muhamad, W.M.A.A. Japar, Z.A. Rasid, An overview of passive techniques for heat transfer augmentation in microchannel heat sink, Int. Commun. Heat Mass Transfer 88 (2017) 74–83.
[13] Z. He, Y. Yan, Z. Zhang, Thermal management and temperature uniformity enhancement of electronic devices by micro heat sinks: A review, Energy 216 (2021) 119223.
[14] A. Arshad, M. Jabbal, Y. Yan, Synthetic jet actuators for heat transfer enhancement – A critical review, Int. J. Heat Mass Transf. 146 (2020) 118815.
[15] G. Hetsroni, M. Gurevich, R. Rozenblit, Sintered porous medium heat sink for cooling of high-power mini-devices, Int. J. Heat Fluid Flow 27 (2) (2006) 259–266.
[16] M.K. Alkam, M.A. Al-Nimr, Solar Collectors with Tubes Partially Filled with Porous Substrates, J. Sol. Energy Eng. 121 (1) (1999) 20–24.
[17] Z.U. Ahmed, M.R. Raihan, O. Ghaffari, M. Ikhlaq, Thermal and Hydraulic Performances of Porous Microchannel Heat Sink Using Nanofluids, J. Therm. Sci. Eng. Appl. 14 (7) (2022).
[18] L. Gong, Y. Li, Z. Bai, M. Xu, Thermal performance of micro-channel heat sink with metallic porous/solid compound fin design, Appl. Therm. Eng. 137 (2018) 288–295.
[19] J.R. Stark, R. Prasad, T.L. Bergman, Experimentally validated analytical expressions for the thermal efficiencies and thermal resistances of porous metal foam-fins, Int. J. Heat Mass Transf. 111 (2017) 1286–1295.
[20] J.R. Stark, C.D. Sevart, T.L. Bergman, Experimentally validated analytical expressions for the thermal resistance of a novel composite fin-foam annular array, Appl. Therm. Eng. 131 (2018) 260–269.
[21] P.C. Huang, K. Vafai, Analysis of forced convection enhancement in a channel using porous blocks, J. Thermophys Heat Transfer 8 (3) (1994) 563–573.
[22] Y. Ould-Amer, S. Chikh, K. Bouhadef, G. Lauriat, Forced convection cooling enhancement by use of porous materials, Int. J. Heat Fluid Flow 19 (3) (1998) 251–258.
[23] P.C. Huang, K. Vafai, Passive alteration and control of convective heat transfer utilizing alternate porous cavity-block wafers, Int. J. Heat Fluid Flow 15 (1) (1994) 48–61.
[24] V.V. Calmidi, R.L. Mahajan, Forced convection in high porosity metal foams, J. Heat Transfer 122 (3) (2000) 557–565.
[25] Y.-T. Yang, C.-Z. Hwang, Calculation of turbulent flow and heat transfer in a porous-baffled channel, Int. J. Heat Mass Transf. 46 (5) (2003) 771–780.
[26] M.L. Hunt, C.L. Tien, Effects of thermal dispersion on forced convection in fibrous media, Int. J. Heat Mass Transf. 31 (2) (1988) 301–309.
[27] H. Xu, Convective heat transfer in a porous-medium micro-annulus with effects of the boundary slip and the heat-flux asymmetry: An exact solution, Int. J. Therm. Sci. 120 (2017) 337–353.
[28] H.J. Xu, Thermal transport in microchannels partially filled with micro-porous media involving flow inertia, flow/thermal slips, thermal non-equilibrium and thermal asymmetry, Int. Commun. Heat Mass Transfer 110 (2020) 104404.
[29] M. Gorzin, A.A. Ranjbar, M.J. Hosseini, Experimental and numerical investigation on thermal and hydraulic performance of novel serpentine minichannel heat sink for liquid CPU cooling, Energy Rep. 8 (2022) 3375–3385.
[30] K. Boomsma, D. Poulikakos, On the effective thermal conductivity of a three-dimensionally structured fluid-saturated metal foam, Int. J. Heat Mass Transf. 44 (4) (2001) 827–836.
[31] I. Kaur, P. Singh, Flow and Thermal Transport Through Unit Cell Topologies of Cubic and Octahedron Families, Int. J. Heat Mass Transf. 158 (2020) 119784.
[32] Z. Wang, M. Zhu, H. Zhang, Y. Zhou, X. Sun, B. Dou, W. Wu, G. Zhang, L. Jiang, Experimental and simulation study on the heat transfer mechanism and heat storage performance of copper metal foam composite paraffin wax during melting process, Energy (2023) 127167.
[33] A. Shahsavar, P. Farhadi, I.B. Askari, Numerical investigation of the effect of perforation inclination angle on the performance of a perforated pin-fin heatsink using two-phase mixture model, Eng. Anal. Bound. Elem. 156 (2023) 488–498.
[34] A. Arshad, M. Ikhlaq, M. Saeed, M. Imran, Numerical analysis of mono and hybrid nanofluids-cooled micro finned heat sink for electronics cooling-(Part-I), International Journal of Thermofluids (2024) 100810.
[35] A. Shahsavar, M. Jafari, Ç. Yıldız, M. Moradvandi, M. Arıcı, On the cooling performance and entropy generation characteristics of a heat sink under ultrasonic vibration: Exploring the impact of porous medium, Int. J. Heat Mass Transf. 215 (2023) 124500.
[36] T. Ambreen, A. Saleem, C.W. Park, Analysis of hydro-thermal and entropy generation characteristics of nanofluid in an aluminium foam heat sink by employing Darcy-Forchheimer-Brinkman model coupled with multiphase Eulerian model, Appl. Therm. Eng. 173 (2020) 115231.
[37] A. Arshad, M. Ikhlaq, M. Saeed, M. Imran, Numerical analysis of mono and hybrid nanofluids-cooled micro finned heat sink for electronics cooling-(Part-II), Therm. Sci. Eng. Prog. 55 (2024) 103005.
[38] L. Chuan, X.-D. Wang, T.-H. Wang, W.-M. Yan, Fluid flow and heat transfer in microchannel heat sink based on porous fin design concept, Int. Commun. Heat Mass Transfer 65 (2015) 52–57.
[39] K. Anirudh, S. Dhinakaran, Numerical study on performance improvement of a flat-plate solar collector filled with porous foam, Renew. Energy 147 (2020) 1704–1717.
[40] S.J. Kim, D. Kim, D.Y. Lee, On the local thermal equilibrium in microchannel heat sinks, Int. J. Heat Mass Transf. 43 (10) (2000) 1735–1748.
[41] X. Zhang, W. Liu, New Criterion for Local Thermal Equilibrium in Porous Media, J. Thermophys Heat Transfer 22 (4) (2008) 649–653.
[42] A. Arshad, M. Jabbal, H. Faraji, P. Talebizadehsardari, M.A. Bashir, Y. Yan, Thermal performance of a phase change material-based heat sink in presence of nanoparticles and metal-foam to enhance cooling performance of electronics, J. Storage Mater. 48 (2022) 103882.
[43] H.-C. Chiu, R.-H. Hsieh, K. Wang, J.-H. Jang, C.-R. Yu, The heat transfer characteristics of liquid cooling heat sink with micro pin fins, Int. Commun. Heat Mass Transfer 86 (2017) 174–180.
[44] M. Ikhlaq, Y.M. Al-Abdeli, M. Khiadani, Nozzle exit conditions and the heat transfer in non-swirling and weakly swirling turbulent impinging jets, Heat Mass Transf. 56 (1) (2020) 269–290.
[45] T. Ambreen, A. Saleem, C.W. Park, Numerical analysis of the heat transfer and fluid flow characteristics of a nanofluid-cooled micropin-fin heat sink using the Eulerian-Lagrangian approach, Powder Technol. 345 (2019) 509–520.
[46] Y. Serkan Şahin, B. İsmet Toprak, İ. Solmaz, Ö. Bayer, Investigation of flow and heat transfer behavior of integrated pin fin-aluminum foam heat sink, Appl. Therm. Eng. 219 (2023) 119504.
[47] T. Ambreen, A. Saleem, C.W. Park, Thermal efficiency of eco-friendly MXene based nanofluid for performance enhancement of a pin-fin heat sink: Experimental and numerical analyses, Int. J. Heat Mass Transf. 186 (2022) 122451.
[48] A. Shahsavar, M. Shahmohammadi, M. Siavashi, CPU cooling with a water-based heatsink filled with multi-layered porous metal foam: Hydrothermal and entropy generation analysis, J. Cent. South Univ. 30 (11) (2023) 3641–3655.
[49] H. Babar, H.M. Ali, Airfoil shaped pin-fin heat sink: Potential evaluation of ferric oxide and titania nanofluids, Energ. Conver. Manage. 202 (2019) 112194.
[50] H. Babar, H. Wu, H.M. Ali, W. Zhang, Hydrothermal performance of inline and staggered arrangements of airfoil shaped pin-fin heat sinks: A comparative study, Therm. Sci. Eng. Prog. 37 (2023) 101616.
[51] A. Li, G. Ahmadi, Dispersion and Deposition of Spherical Particles from Point Sources in a Turbulent Channel Flow, Aerosol Sci. Tech. 16 (4) (1992) 209–226.